



Effects of plastic constraint on the cyclic and static fatigue behavior of metal/ceramic layered structures

J.J. Kruzic, J.M. McNaney, R.M. Cannon, R.O. Ritchie *

*Materials Sciences Division, Lawrence Berkeley National Laboratory, Department of Materials Science and Engineering,
University of California, Berkeley, CA 94720, USA*

Received 30 December 2001; received in revised form 31 January 2002

Abstract

The role of metal layer thickness and resultant plastic constraint in the metal layer during the failure of metal/ceramic layered structures is examined under cyclic and static loading conditions. Crack-growth experiments were conducted on sandwich specimens consisting of 99.999% pure aluminum layers bonded between 99.5% pure polycrystalline alumina with the metal layer thickness varying from 5 to 100 μm . Under cyclic loading, crack growth occurred primarily at the interface separating the two materials; additionally, stable fatigue cracks deviated into the alumina for thin-layered samples at high driving forces. Under monotonically increasing loads, the fracture toughness *increased* with Al layer thickness, whereas under cyclic loads the threshold driving force for crack growth conversely *decreased* with increasing layer thickness. Under static loading in a moist environment, interfacial crack growth was never observed at measurable rates ($\geq 10^{-9}$ m/s) for driving forces up to 200 J/m²; however, for thin-layered samples, subcritical cracks did deviate off the interface and grow, sometimes stably, into the alumina. Trends in crack-growth rates and crack trajectories are examined in terms of the level of constraint, loading conditions and environmental influences.

© 2003 Elsevier Ltd. All rights reserved.

Keywords: Interface fracture; Fatigue-crack growth; Stress-corrosion cracking; Plastic constraint; Alumina; Aluminum

1. Introduction

Metal/ceramic interfaces play a crucial role in dictating the mechanical properties of reinforced and layered structures used in many engineering applications, including microelectronic packaging, multi-layered films, coatings, joints, and composite materials. The design of reliable engineering sys-

tems requires that the structural integrity of such interfaces be maintained during the lifetime of the component. Research focused on the strength and fast fracture behavior of metal/ceramic interfaces in ceramic/metal/ceramic sandwich structures has been extensive (Dalglish et al., 1988, 1989, 1994; Korn et al., 1992; Ellsner et al., 1985; Evans and Lu, 1986; Evans et al., 1989; Evans and Dalglish, 1992; Reimanis et al., 1991; Suo and Hutchinson, 1989; Turner and Evans, 1996; McNaney et al., 1994; Varias et al., 1991). While a handful of studies have reported on the corresponding subcritical crack-growth properties, specifically involving

* Corresponding author. Tel.: +1-510-486-5798; fax: +1-510-486-4995/+1-510-486-4881.

E-mail address: roritchie@lbl.gov (R.O. Ritchie).

cyclic fatigue-crack growth (Shaw et al., 1994; McNaney et al., 1996; Gaudette et al., 1999; Cannon et al., 1991; Peralta et al., 2000) and static fatigue by moisture-assisted (stress-corrosion) cracking (Oh et al., 1987, 1988; Reimanis et al., 1990; Card et al., 1993), surprisingly few results on crack propagation at, or near, bimaterial interfaces are available.

In the study of interfacial and near-interfacial crack propagation, ceramic/metal/ceramic sandwich structures provide additional complexity over bimaterial interfaces due to additional constraint of the plasticity in the metal layer by the surrounding ceramic. Indeed, the level of constraint of the plastic zone ahead of the crack tip imposed by surrounding elastic material is always a concern, even when applying fracture mechanics to monolithic materials. For example, the constraint associated with the thickness of the sample, i.e., whether plane strain or plane stress conditions exist, is known to have a profound effect on toughness properties. Additionally, loss of constraint can occur if plasticity extends to a free surface of a sample (e.g., the back face), again affecting the measured properties. In the case of a ductile layer between ceramic members, additional constraint of the plastic zone may occur when plasticity extends across the thickness of the metal layer, impinging on the ceramic (Fig. 1). Furthermore, constraint through the layer is significantly affected by the metal layer thickness; in fact, theoretical studies have shown that the plastic-zone size, crack-tip opening displacement (CTOD) and the stress-state near a crack tip are all affected by variations in the layer thickness (Varias et al., 1991).

Despite the importance of this topic, there have been relatively few experimental investigations on how failure mechanisms in bimaterial layered systems are affected by changes in plastic constraint, achieved through variations in the metal layer thickness (Ashby et al., 1989; Reimanis et al., 1991; McNaney et al., 1996; Dalgleish et al., 1989, 1994; De Graef et al., 1992), with only the work of McNaney et al. (1996) focusing (in part) on fatigue failure. Trends of *increasing* strength with decreasing layer thickness in several metal/ Al_2O_3 systems have been observed (Dalgleish et al., 1989,

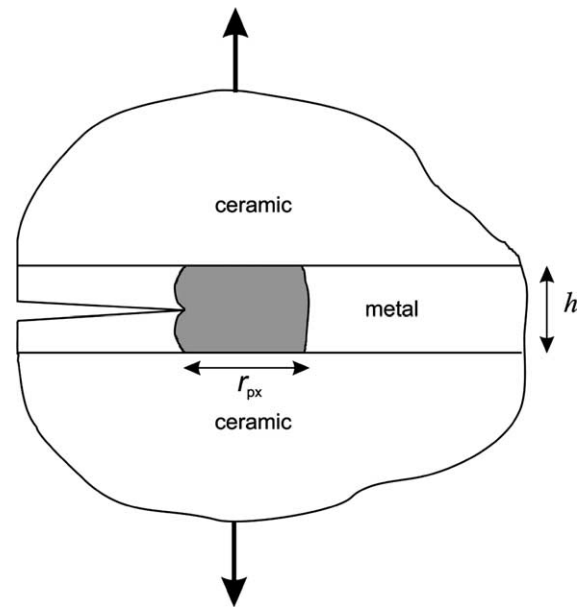


Fig. 1. Schematic illustrating constraint of the plastic zone ahead of a crack tip which extends through the thickness of a metal layer bonded between two ceramic members.

1994), whereas investigations using 10–125 μm thick layers of gold or platinum bonded between sapphire show a clear trend of *decreasing* fracture toughness with decreasing layer thickness (Reimanis et al., 1991; De Graef et al., 1992); such trends in toughness were not as definitive in the Al/ Al_2O_3 system, however, where the layer thickness ranged from 100 to 500 μm (McNaney et al., 1996). While crack-tip blunting profiles indicated this definitive trend of lower toughness values at smaller layer thicknesses, the effect could not be clearly demonstrated with conventional linear-elastic fracture mechanics, i.e., K_c measurements due to excessive plasticity and possible loss of plastic constraint at the back face of the specimen, both from the high interfacial toughness and low metal yield strength of the Al/ Al_2O_3 system (McNaney et al., 1996).

Since strength increases with decreasing layer thickness in the aluminum/alumina system, whereas the (large crack) fracture resistance appears to decrease, compromise is needed to achieve a suitable balance of properties for any given application. It is additionally important for time- or cycle-

dependent applications that the trends in fatigue resistance with changing layer thickness (and consequently plastic constraint) are understood and incorporated into the design of systems for the optimum performance. In this regard, prior work on the Al/Al₂O₃ system using 100–500 μm thick layers indicated that cyclic loading led to predominantly interfacial failure in an apparently ductile manner (via ductile fatigue striations), although no effects of layer thickness were observed (McNaney et al., 1996). However, for further reductions in the metal layer thickness, an effect on fatigue-crack growth rates may be expected due to constraint of the plastic zone from the impinging ceramic (Fig. 1). Specifically, since cyclic fatigue-crack growth in ductile materials is dependent on plastic deformation mechanisms near the crack tip, a retardation of fatigue-crack growth mechanisms may be expected from the restriction in dislocation motion by the metal/ceramic interface.

Changes in the metal layer thickness are also expected to affect the static fatigue properties. While no evidence of moisture-assisted slow crack growth under static loading has been previously found for the aluminum/alumina system (McNaney et al., 1996), such behavior has been observed for sapphire/gold (Reimanis et al., 1990), sapphire/nickel (Gaudette et al., 1997), and glass/copper (Card et al., 1993; Oh et al., 1987) interfaces in sandwich specimens. Moreover, both single and polycrystalline alumina are prone to such moisture-assisted cracking in humid environments (Evans, 1972; Wiederhorn, 1968), such that it might be anticipated that Al₂O₃/Al/Al₂O₃ sandwich samples would similarly be susceptible, either at the interface or in the alumina, if adequate local crack-tip stresses are achieved.

Accordingly, in this work, we present cyclic fatigue results for Al₂O₃/Al/Al₂O₃ sandwich samples with 5–100 μm thick aluminum layers and examine how changes in the metal layer thickness can affect cyclic fatigue-crack propagation rates at and near the interface. In addition, the moisture-assisted slow crack-growth properties of these samples are studied, as it is anticipated that the increasing constraint will limit crack-tip blunting, thereby raising local crack-tip stresses and activating differing failure mechanisms.

2. Experimental procedures

Sandwich specimens with 5, 35, and 100 μm thick layers of 99.999% pure aluminum bonded between 99.5% pure polycrystalline Coors AD995 alumina were fabricated by liquid state bonding. The alumina microstructure has grain sizes ranging from ~ 1 to 50 μm with a measured mean linear intercept of 12 μm , corresponding to an average grain size of $d_g \approx 18 \mu\text{m}$. Blocks of alumina (21.3 mm square by 10.2 mm thick) were lapped flat to a 1 μm finish and carefully cleaned in acetone and ethanol before baking at 1000 $^{\circ}\text{C}$ for 1 h to remove organic impurities. High purity (99.999%) aluminum foils (100 and 35 μm thick layers) or evaporated coatings (5 μm thick layers) were placed between two alumina blocks and cold pressed to ~ 40 MPa before placing in a closed, high purity alumina crucible for bonding. Sandwich assemblies were heated to a temperature of 980 $^{\circ}\text{C}$ in a gettered argon environment and held for 5 min before cooling. Further processing details are given elsewhere by Dalgleish et al. (1989). Bonded blocks were machined into compact tension, $C(T)$, specimens ($B = 3$ mm, $W = 14$ –17 mm, $a_0 = 5$ mm) for mechanical testing (Fig. 2). For comparison, monolithic alumina $C(T)$ samples were also machined in order to characterize the fracture and fatigue-crack growth properties of the bulk alumina.

Cyclic fatigue-crack growth rates were measured in room air at 25 $^{\circ}\text{C}$ (20–40% relative humidity) in

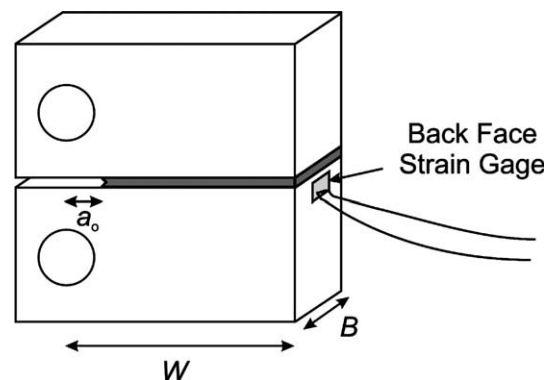


Fig. 2. Schematic illustration of the sandwich compact-tension, $C(T)$, specimen.

general accordance with ASTM standard E647. Tests were conducted at a frequency of 25 Hz (sine wave) using computer-controlled servo-hydraulic testing machines at a positive, constant load ratio (ratio of minimum to maximum loads) of $R = 0.1$. Crack lengths were continuously monitored by compliance methods using strain gauges mounted on the back face of the specimen, specifically on the alumina adjacent to the aluminum layer (Fig. 2). Standard $C(T)$ compliance calibrations for monolithic samples were used (Deans and Richards, 1979), which proved to be accurate for the present sandwich $C(T)$ samples (as verified by periodic optical measurements), even in the presence of crack jumping from interface to interface. Crack-driving forces were assessed using the range of strain energy release rate, $\Delta G = G_{\max} - G_{\min}$. For the samples used in this study, where the layer thickness, h , is small compared to all other relevant sample dimensions, the strain energy release rate, G , is essentially unaffected by the presence of the layer (Suo and Hutchinson, 1989). G can be calculated from standard linear-elastic stress–intensity solutions for monolithic samples, K_I^∞ , using the relationship:

$$G = \frac{K_I^{\infty 2}}{E'} \quad (1)$$

where $E = E$ in plane stress and $E/(1 - \nu^2)$ in plane strain, E is Young's modulus for alumina, and ν is Poisson's ratio. Fatigue-crack growth rate versus applied driving force (i.e., $da/dN - \Delta G$) curves were assessed using both increasing and decreasing loading schemes (i.e., under increasing and decreasing ΔG conditions); the latter method was used to obtain ΔG_{TH} fatigue thresholds, that were defined as the applied ΔG corresponding to growth rates below $\sim 10^{-10}$ m/cycle. Specifically, cracks were initiated by cycling until stable interface cracks formed ahead of the machined notches. Then, the loads were either incrementally reduced to measure the behavior approaching the threshold or increased to obtain the high velocity portion of the crack-growth curves. For practical considerations, tests were controlled using the far-field applied stress–intensity range, ΔK_I^∞ , utilizing continuous load shedding that limited the ΔK_I^∞ -gradient ($= 1/\Delta K_I^\infty [d\Delta K_I^\infty/da]$) to $\pm 0.08 \text{ mm}^{-1}$.

Ideally, this rate of change in loads was sufficiently slow to allow the crack blunting or bridging levels to adjust to the current load and level of ΔK_I^∞ or ΔG , i.e., the increment in crack extension at each load level exceeded several plastic-zone sizes, the latter being estimated from the results of Varias et al. (1991).

After fatigue testing, fracture toughness tests were performed on the fatigue-cracked $C(T)$ samples to assess trends in fracture toughness with changing layer thickness. Toughness values were characterized in terms of the critical strain energy release rate, G_c calculated from the peak loads at failure using Eq. (1).

Moisture-assisted crack growth (static fatigue) experiments were conducted on fatigue pre-cracked $C(T)$ specimens in a controlled high humidity (>95% relative humidity) room air environment, with the fatigue pre-cracks initially located at the interface. High humidity conditions were maintained by bubbling room air twice through distilled water and into a closed testing chamber. Samples were tested under constant load, i.e., with increasing crack-driving forces. To determine crack velocity, da/dt , crack lengths, a , were monitored in situ using the back-face strain signal to estimate the unloading compliance curve. Additionally, crack lengths were periodically verified by the more accurate method of unloading the sample and measuring the actual unloading compliance. Samples were initially held at loads where reasonably measurable growth rates ($da/dt > 10^{-9}$ m/s) could not be achieved. Loads were then step increased and held until measurable growth could be detected at some constant load, at which point all tests were conducted using an increasing loading scheme due to the increasing G field associated with constant loading for the $C(T)$ geometry. When possible, samples were unloaded before critical fracture occurred.

3. Results and discussion

3.1. Fracture toughness properties

A definitive trend of increasing toughness with increasing aluminum layer thickness, over the

range of 5–100 μm , was found for the fatigue pre-cracked $\text{Al}_2\text{O}_3/\text{Al}/\text{Al}_2\text{O}_3$ sandwich samples (Fig. 3). For all samples tested, the fatigue pre-crack, which was located at the interface, was observed to initiate brittle failure in the alumina, with the $\text{Al}_2\text{O}_3/\text{Al}$ interface remaining intact. Although fracture occurred in the ceramic, fracture toughness values for the interface samples were well in excess of the initiation toughness of $\sim 20 \text{ J/m}^2$ taken from the measured crack-resistance curve (R -curve) for bulk polycrystalline alumina (Fig. 4). As fracture in the alumina depends on the stresses in the ceramic near the interface crack tip, the large increase in toughness, compared to that of bulk alumina, may be attributed to lower crack-tip stresses due to crack blunting in the aluminum.

Fig. 5 shows direct evidence of this blunting phenomenon based on in situ images, taken in a field emission scanning electron microscope (FESEM), of a sandwich $C(T)$ sample just prior to ultimate failure at 346 J/m^2 . The tip of the fatigue crack at the interface of a $100 \mu\text{m}$ thick layer sample was observed to blunt into the aluminum

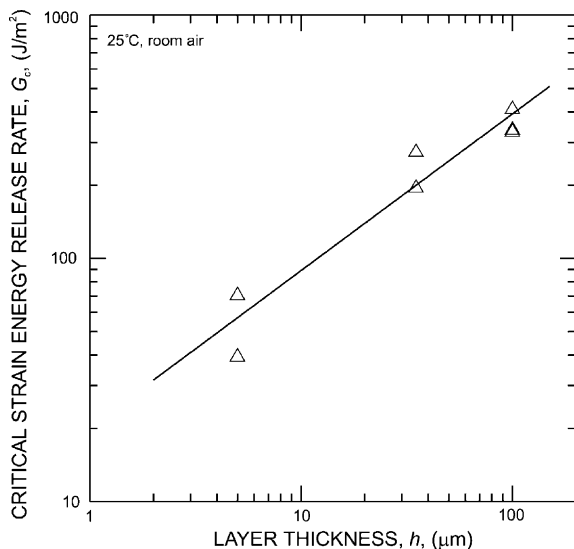


Fig. 3. Fracture toughness results for polycrystalline alumina/aluminum/alumina sandwich specimens as a function of metal layer thickness. All samples failed in the alumina.

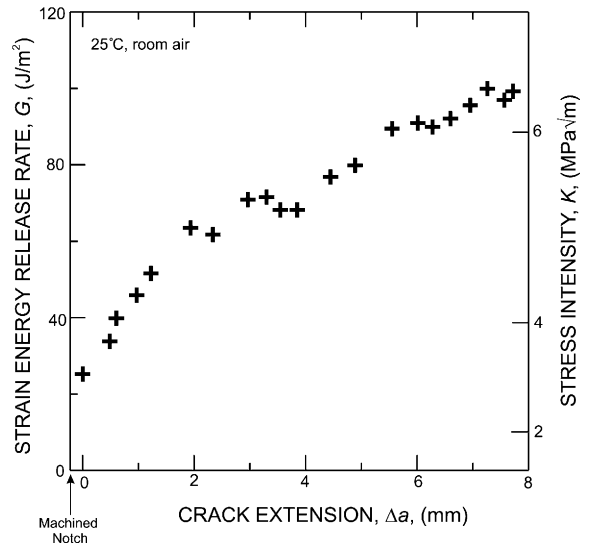


Fig. 4. R -curve measured for Coors AD995 alumina demonstrating rising crack-growth resistance with crack extension. Data shown were collected from a fatigue pre-cracked $C(T)$ sample where the pre-crack was grown only $230 \mu\text{m}$ from the machined notch to minimize the bridging that was generated during initial crack formation.

during loading from 76 to 280 J/m^2 . The measured CTOD for this sample increased due to plastic deformation in the aluminum from sub-micron levels up to $\sim 2.6 \mu\text{m}$ at 280 J/m^2 . Based on linear-elastic fracture mechanics, local stresses near a blunted crack/notch (Fig. 5) are considerably lower than those ahead of a sharp crack tip at the same applied driving force. For example, using the linear-elastic solutions of Creager and Paris (1967) to calculate the stresses ahead of a blunt crack/notch with root radius ρ in an isotropic, monolithic material, it can be shown that for any given applied driving force the crack-opening stresses, σ_{yy} , are reduced by 42% and 22% relative to the sharp crack case at distances of $\rho/20$ and $\rho/10$ ahead of the crack tip, respectively. Thus, in the case of the blunted interface cracks, a larger applied driving force is necessary to achieve the stresses necessary to initiate fracture of the alumina, thereby giving a higher measured fracture toughness for the sandwich specimens, compared to that for bulk alumina.

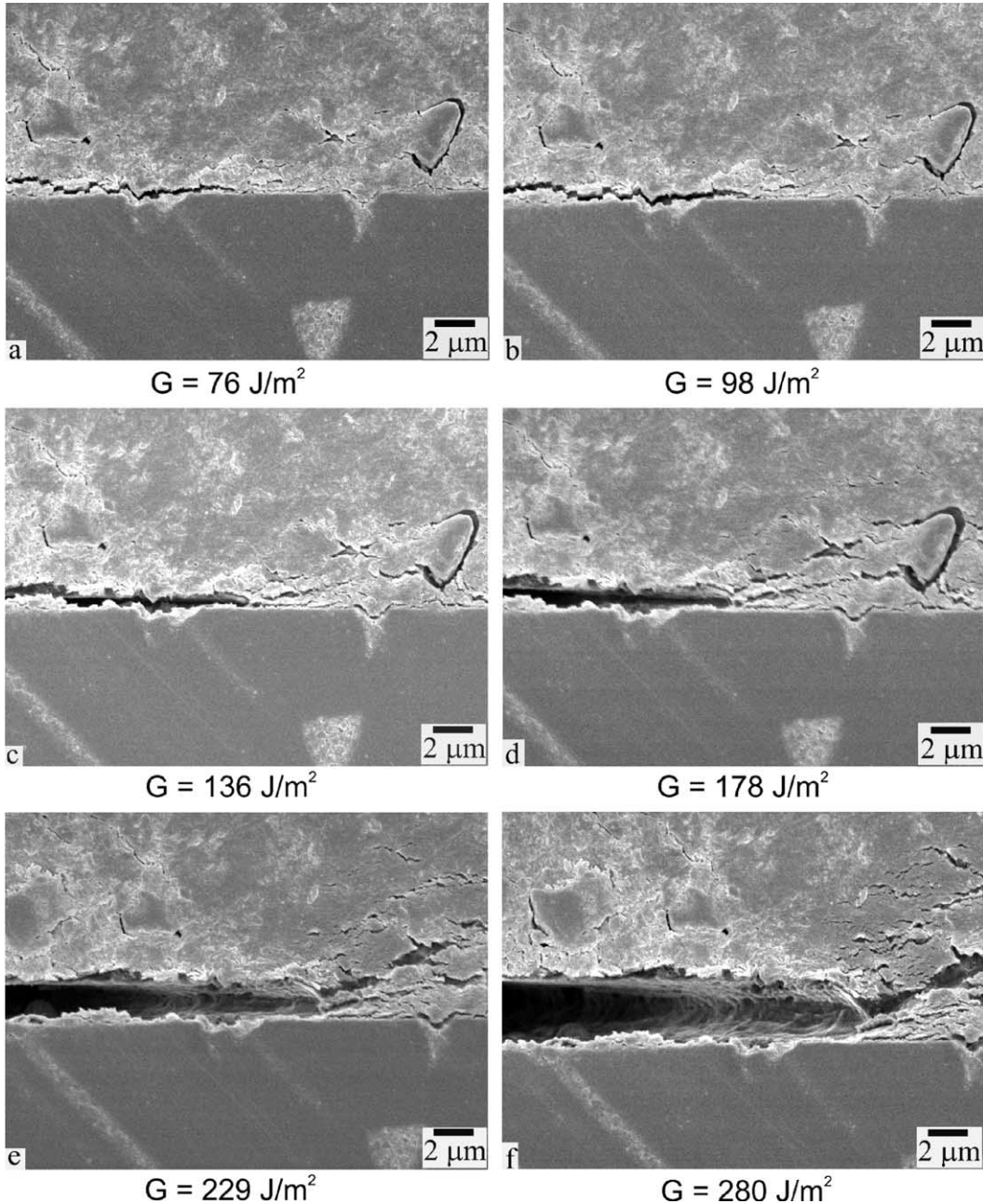


Fig. 5. Blunting of an interfacial crack into a 100 μm thick aluminum layer during in situ loading in the FESEM as the applied driving force was increased from 76 to 280 J/m^2 . The sample failed at an applied driving force of 346 J/m^2 in the adjoining alumina.

The observed trend of increasing toughness with increasing layer thickness can also be attributed to greater crack-tip deformation and blunting

due to diminished plastic constraint through the thickness of the metal layer. To evaluate whether plastic deformation will impinge on the opposite

alumina piece and become constrained, plastic-zone size estimates¹ were made for a crack at a bimaterial interface, where plasticity can extend into the aluminum unconstrained. Using the results of Shih and Asaro (1988, 1989), the distance, r_{py} , that the plastic zone extends into the aluminum, normal to the interface, can be predicted. Estimates reveal that the plastic zone would extend $\sim 100 \mu\text{m}$ into the aluminum (i.e., comparable to the thickest layers of this study) at a driving force of only $\sim 11 \text{ J/m}^2$. For all cases tested in this study, this implies that at the driving forces necessary for fracture ($>40 \text{ J/m}^2$), the plastic zone extends across the entire thickness of the aluminum layer, thereby limiting the amount of plasticity, and in turn the crack-tip blunting, that can occur. For samples with thin layers, blunting is limited by the metal layer thickness at relatively low driving forces, leading to sharper crack tips than in samples with thicker layers. This constraint also results in higher triaxial stresses ahead of the crack tip. To illustrate this, the maximum mean, or hydrostatic, stress, defined as $\sigma_m = 1/3(\sigma_{xx} + \sigma_{yy} + \sigma_{zz})$, normalized by yield stress, σ_0 , ahead of the crack tip can be used. Indeed, the computed maximum value of σ_m/σ_0 ahead of the crack tip reaches a level of 6.65 at an applied driving force of ~ 15 and $\sim 295 \text{ J/m}^2$ for 5 and 100 μm thick layer samples, respectively. These values derive from computations of Varias et al. (1991) for the centerline crack configuration (Fig. 1); while that geometry is slightly different from the present one, the predictions are reasonably sound for interface cracks where plasticity extends across the entire layer, and well ahead of the crack tip, and accordingly preserve the qualitative trends for the present case. Thus, it is concluded that at the same applied driving force, samples with thinner, more highly constrained, layers experience higher local stresses ahead of the (sharper) crack tip. Accordingly, for samples with thinner aluminum layers, flaws in the alumina ahead of the crack tip can be more easily triggered, and fracture in the alumina can occur more readily, due to the more severe stress-state.

Additionally, it should be noted that for the samples with 100 μm , and perhaps 35 μm , layer thicknesses, the G_c toughness values calculated from asymptotic stress–intensity solutions may underestimate the total fracture energy due to excessive plasticity in the aluminum, i.e., from a violation of small-scale yielding assumptions. Computed plastic-zone size estimates in the direction ahead of the crack tip, r_{px} indicate that at a driving force of 280 J/m^2 , the plastic zone already extends $>1 \text{ mm}$ ahead of the crack tip for $h = 100$ and 35 μm (Varias et al., 1991), which is not small compared to sample dimensions. Indeed, the work of McNaney et al. (1996) showed that for layer thicknesses $\geq 100 \mu\text{m}$, large-scale plasticity with associated load-point displacements account for a significant fraction of the fracture energy; consequently, no trend of decreasing fracture toughness with decreasing layer thickness could be determined when driving forces were calculated using linear-elastic solutions. In the present study, however, although predicted plastic-zone sizes for 100 and 35 μm thick layer samples are large in one dimension, all samples demonstrated essentially linear load–displacement curves to failure. This strongly implies that deviations from small-scale yielding conditions are most likely small as a result of constraint of the plastic zone through the thickness of the layer. Additionally, for samples with 5 μm thick layers, the plastic-zone size is limited to sizes relatively small compared to sample dimensions; this is due to increased constraint and low toughness such that small-scale yielding assumptions are considered valid. Accordingly, in contrast to the work of McNaney et al. (1996), trends of decreasing fracture energy are observed when using the present linear-elastic fracture mechanics solutions. Indeed, the trend seen in Fig. 3 may be anticipated to be even more pronounced if large-scale plasticity were taken into account in the calculation of the crack-driving forces for the thicker layer samples.

3.2. Cyclic fatigue-crack growth properties

3.2.1. Interfacial cyclic fatigue-crack growth

In contrast to the fracture toughness properties, a trend of increasing crack-growth resistance with

¹ A flow stress of 50 MPa for the aluminum was used for all plastic-zone size calculations in this paper.

decreasing aluminum layer thickness was observed for cyclic fatigue of the $\text{Al}_2\text{O}_3/\text{Al}/\text{Al}_2\text{O}_3$ sandwich samples in the near-threshold regime (Fig. 6); crack propagation occurred exactly at the interface for all results in Fig. 6. Samples with 5 μm thick layers showed a factor of two higher fatigue thresholds than the 100 μm thick layer samples, as well as an order of magnitude lower growth rates at comparable driving forces in the near-threshold regime, while samples with 35 μm thick layers exhibited intermediate behavior in both regards. Data from McNaney et al. (1996), for samples with 100–500 μm thick layers where no such trend was observed, are also shown for comparison.

Fatigue striations were observed on the aluminum side of the fracture surface, as reported by McNaney et al. (1996), suggesting a mechanism of fatigue-crack propagation similar to that in ductile metals, i.e., crack advance occurred by a process that involves blunting and resharping of the crack tip, with individual striation markings corresponding to each blunting event. The amount of crack advance per cycle is typically directly related to the amount of blunting at the crack tip, with the cyclic growth increment typically scaling with

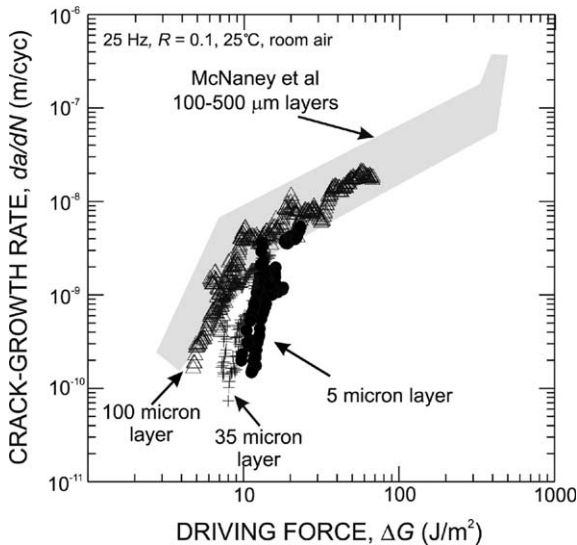


Fig. 6. Fatigue-crack growth results for interfacial cracks showing an increase in crack-growth resistance with decreasing layer thickness in the near-threshold regime. Additional data from McNaney et al. (1996).

some fraction of the CTOD, e.g., ~ 0.1 – 0.3 for mode I self-similar growth in ductile metals (Gu and Ritchie, 1999). Thus, if plastic constraint restricts the degree of blunting during each cycle, this should act to reduce the growth rate for samples with thinner layers. While this gives rise to higher fatigue resistance in the more highly constrained samples, it is important to note that for layer thicknesses $\geq 100 \mu\text{m}$, the computed plastic-zone width, r_{py} at the crack tip is small enough near the fatigue threshold ($\sim 35 \mu\text{m}$ at 4 J/m^2 (Shih and Asaro, 1988, 1989)) so that it does not extend completely across the metal layer. In this range of layer thicknesses, no effect of layer thickness is to be expected; indeed, experiments by McNaney et al. (1996) observed no layer thickness effects on fatigue thresholds and velocities under cyclic loading in the range of 100–500 μm thick aluminum layers.

Examination of the fatigue surface of 5 μm thick layer samples after failure revealed a crack path alternating between one interface and the other during fatigue-crack growth (Fig. 7a). While macroscopic jumps of the entire crack front from one interface to another were not uncommon for all samples, the additional localized jumps seen in Fig. 7a, distributed across the fatigue surface, were unique to 5 μm thick layer samples. Observations of crack profiles in unbroken samples (Fig. 7b) revealed such jumping to be initiated predominantly at flaws in the alumina microstructure. In Fig. 7b the crack, originally propagating on the upper interface, reinitiated on the other side of the layer at a flaw in the alumina; it then grew to, and propagated along, the lower interface. Crack jumping from interface to interface can potentially lead to bridging ligaments of aluminum in the crack wake, which may sustain some applied load and result in an increased fatigue threshold (Cannon et al., 1991); however, a recent study of the fatigue behavior of 2 μm thick layers of 99.999% aluminum between sapphire members, wherein smaller flaws exist and no crack jumping was reported, defined a fatigue threshold of $\sim 10 \text{ J/m}^2$ (Gaudette et al., 1999). This value is similar to results for the 5 μm thick layer samples and significantly higher than the threshold of 4 J/m^2 found for 100 μm thick layer samples in the pre-

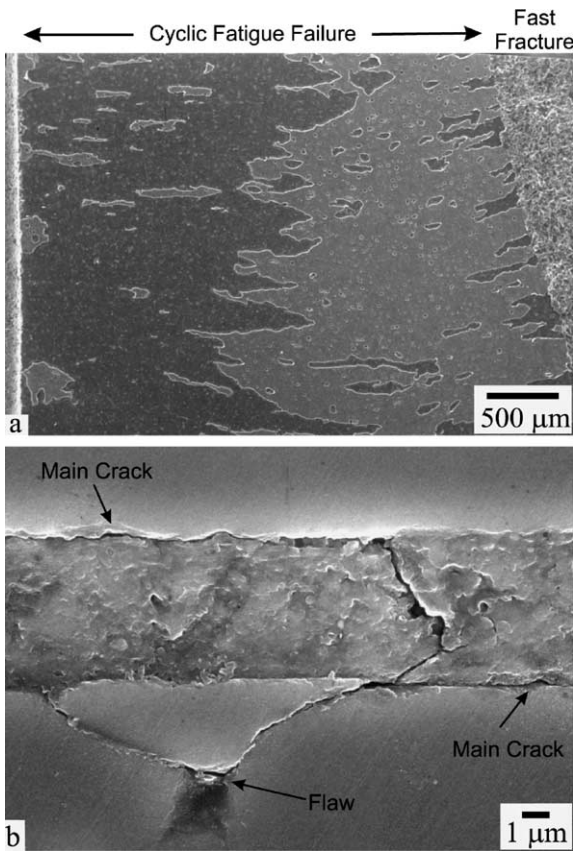


Fig. 7. Evidence of crack jumping both (a) on the fatigue fracture surface and (b) in profile on a 5 μm thick layer sample. In (a) aluminum is seen in lighter contrast on the fatigue fracture surface. Crack jumping is observed to initiate at flaws in the alumina. Direction of crack propagation was left to right with respect to the micrographs.

sent work, suggesting that effects on the fatigue threshold due to crack jumping are secondary to that of plastic constraint.

3.2.2. Deviation of cyclic fatigue cracks into the alumina

At higher driving forces in samples with 5 μm thick layers, cyclic fatigue cracks were observed to leave the interface and grow into the alumina; data for the stable crack growth in the alumina are represented by open symbols in Fig. 8. Crack initiation and growth into the alumina for these samples is attributed to the higher local crack-tip stresses (due to plastic constraint through the metal

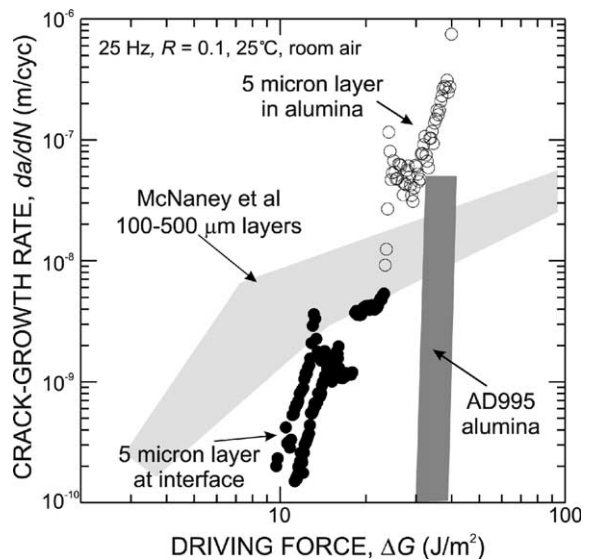


Fig. 8. Fatigue-crack growth rate results for a fatigue crack leaving the interface of a 5 μm thick layer sample and growing stably in the alumina. Growth rates were initially faster than that in bulk alumina, with the data merging only after >2 mm of crack extension.

layer) than would occur for thicker metal layers ($h \geq 100 \mu\text{m}$). Many alumina ceramics, including Coors AD995, display a true cyclic fatigue effect, with degradation of the grain bridges being attributed as the salient mechanism for crack advance (Lathabai et al., 1991; Geraghty et al., 1999; Gilbert et al., 1995; Guiu et al., 1992; Dauskardt, 1993). Under monotonic loading, when intergranular fracture is predominant in alumina, frictional tractions along the fractured grain boundaries in the crack wake sustain load and shield the crack tip from part of the applied driving force, resulting in rising toughness with crack extension as these bridges develop (Swanson et al., 1987; Mai and Lawn, 1987; Bennison and Lawn, 1989). Evidence of this behavior can be seen in the rising *R*-curve shown in Fig. 4. As the crack is cycled open and closed, however, the grain bridges that provide for toughening in the alumina degrade by mechanisms such as frictional wear at the grain boundaries, thereby raising the effective driving force at the crack tip and hence promoting crack advance.

For the present 5 μm thick layer samples, after the crack leaves the interface and enters the

alumina, cracking occurs at higher growth rates than is typically measured for bulk alumina over the first ~ 2 mm of growth (Fig. 8). Since alumina demonstrates rising *R*-curve behavior under monotonic loading (Fig. 4), it is not surprising to observe crack size effects under cyclic loading as well. An effect of crack size in fatigue is typically referred to as a short or small crack² effect, with short cracks generally growing at rates faster than long cracks at the same *applied* driving force (e.g., Ritchie and Yu, 1986). With ceramics, cracks may be considered to be short if the crack length is smaller than the distance over which extrinsic toughening (crack-tip shielding) takes place behind the crack tip. Crack size effects have been observed for small surface cracks in both alumina (Healy et al., 1997; Kishimoto et al., 1998), and other grain-bridging ceramics (Steffen et al., 1991; Gilbert et al., 2000; Zhang and Edwards, 1996), with these effects attributed to such extrinsic mechanisms as reduced grain bridging and compressive residual stresses.

While in the present case the interfacial cracks are physically long, alumina grain bridges (Fig. 9) can only begin to develop and sustain load after the crack has entered the alumina. The observed behavior is shown by the open symbols in Fig. 8, where after the initial spike in growth rates corresponding to the change from an interfacial to alumina crack path, crack-growth rates are then reduced before increasing again so the data merge with the standard large-crack fatigue data; this results in a V-shaped da/dN – ΔG curve, which is characteristic of short crack fatigue behavior observed in many extrinsically toughened materials including AD995 alumina (e.g., Kruzic et al., 1999, 2003; Andreasen et al., 1995; Gilbert et al., 2000). This apparently anomalous behavior can be explained as follows: as the crack grows into the

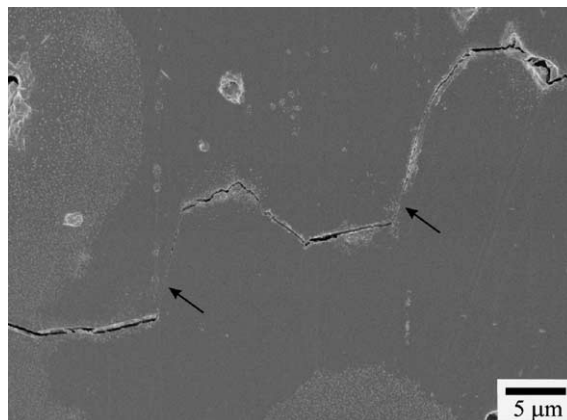


Fig. 9. Evidence of frictional grain bridging in the wake of a fatigue crack growing in the alumina. Arrows indicate points of frictional contact in the crack wake. Direction of crack propagation was left to right with respect to the micrograph.

alumina, although the applied driving force is increasing, crack-tip shielding due to the grain bridges initially increases at a faster rate, causing the effective driving force at the crack tip to decrease; this leads to an initial reduction in crack-growth rates. After further crack growth, however, a steady-state is reached where grain bridges are created and degraded at an equal rate, and the growth rates match those of the large cracks in the bulk alumina.

Bridging zones associated with cyclic fatigue-crack growth in the alumina were observed in the present study to be on the order of 2 mm, based on the convergence point of the near interfacial and long-crack alumina data (Fig. 8). Under monotonic loading, rising crack resistance is still observed after more than 8 mm of crack growth (Fig. 4), which suggests an equilibrium bridging zone greater than 8 mm in length. Clearly this is much greater than the 2 mm zone observed in fatigue, which supports the notion that it is indeed the degradation of the bridging zone under cyclic loading that is responsible for fatigue-crack growth in alumina ceramics. Additional experimental evidence of smaller equilibrium bridging zones under cyclic, as compared to monotonic, loading has been reported for alumina by Hu and Mai (1992).

Furthermore, a rough estimate of the bridging-zone length under monotonic loading can be made

² Short or small fatigue cracks are defined as cracks small compared to: (i) the scale of microstructure, (ii) the extent of local inelasticity, or (iii) the extent of crack-tip shielding in the crack wake, where short cracks are small in one dimension and small cracks are small in all dimensions. They can generally grow at rates in excess of corresponding large cracks due to a higher local (near-tip) driving force experienced at the crack tip, e.g., Suresh and Ritchie (1984).

by noting that effective grain bridging occurs only up to the point behind the crack tip where the crack-opening displacement is approximately 1/4 to 1/3 of the average grain size, d_g (Hay and White, 1993; Steinbrech et al., 1987). Using a simple hinge model for crack opening, the extent of the grain-bridging zone can thus be estimated by calculating the point where the crack opening is approximately in this range. The opening displacement at the loadline, δ , is given by

$$\delta = \frac{P}{E'B} V\left(\frac{a}{W}\right) \quad (2)$$

where P is the applied load, B and W are the specimen thickness and width, respectively, and the function $V(a/W)$ is tabulated in Saxena and Hudak (1978). Although Eq. (2) was developed for monolithic $C(T)$ specimens, the numerical results of McNaney et al. (1997) indicate that for thin layer sandwich $C(T)$ specimens, differences in the load-line displacement are small (<10%) for all crack lengths, and thus Eq. (2) can be used here for simplicity. While the axis of rotation for an unbridged, linear-elastic crack is typically taken as $0.2(W - a)$ ahead of the crack tip (Veerman and Muller, 1972), experimental observations by Steinbrech et al. (1987) on alumina specimens suggest that grain-bridging interactions across the crack faces draw the axis of rotation very near to the crack tip with the crack faces opening in a linear manner. Thus, taking the hinge of rotation to be at the crack tip, and assuming a linear crack-opening profile from the crack tip to the loadline, the rule of similar triangles can be used to determine the point where the crack opening is approximately $d_g/4 - d_g/3$. Using this method, a grain-bridging zone extending some 8–11 mm behind the crack tip under monotonic loading can be calculated for the present Coors AD995 alumina, a figure that is consistent with the present R -curve results and significantly larger than the 2 mm cyclic bridging zone inferred from experimental fatigue results. Using this model, a bridging zone length of ~ 2 mm for cyclic loading implies that effective grain bridges exist behind the crack tip up to the point where the crack opening is on the order of $d_g/16$, which may be a useful parameter for future predictions of bridging-zone lengths

under cyclic loading in grain-bridging alumina ceramics.

In the present study, two distinct crack trajectories have been observed under cyclic loading for a crack initially at the Al/Al₂O₃ interface. In addition to the interfacial crack path, under conditions of high loading and plastic constraint, it has been found that the cracks may leave the interface and propagate stably into the alumina under cyclic loading. Such behavior was seen to occur at driving forces of $\Delta G \approx 23$ J/m² for 5 μ m thick layer samples (Fig. 8). Additionally, due to crack size effects, initial crack propagation in the alumina for interface samples with thin metal layers occurs at driving forces lower than necessary for propagation of large cracks in bulk alumina. While thinner, more highly constrained, layers show improved fatigue properties in the near-threshold regime, the change in fatigue mechanism from ductile fatigue at the interface to brittle fatigue in the alumina at higher driving forces, coupled with the short-crack effects, means that the samples with thin layers have inferior fatigue resistance at increased driving forces.

3.3. Moisture-assisted crack-growth properties

For cracks in Al₂O₃/Al/Al₂O₃ sandwich samples under static loading in a moist environment (>95% relative humidity), separation along the Al₂O₃/Al interface was not observed in any of the samples tested. Stable crack growth did occur, however, in samples with thinner aluminum layers when interfacial fatigue pre-cracks left the interface to propagate into the alumina. As shown in Fig. 10, initial crack growth in the alumina for the 5 μ m thick layer samples occurred at driving forces that were lower than necessary for equivalent growth in fatigue pre-cracked bulk alumina samples. For samples with 35 μ m thick aluminum layers, analogous crack growth occurred in two of three samples, but only at driving forces larger than necessary to crack bulk alumina. Due to the high driving forces necessary to initiate growth into the alumina in these samples, once the crack had grown a short distance from the plastically deforming aluminum layer, catastrophic fracture occurred, limiting the amount of subcritical

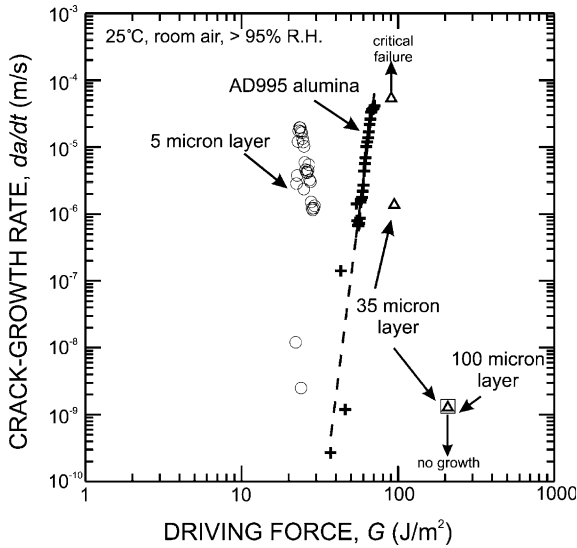


Fig. 10. Moisture-assisted crack-growth rates for interface and bulk alumina specimens in moist air (>95% relative humidity). Crack growth was in the alumina for interface samples where discernible cracking occurred.

crack-growth data that could be obtained. It should be noted that this was a true time-dependent effect, with failure occurring only after several hours at constant load. Indeed, limited stable crack growth was sometimes actually measured before final failure, as shown in Fig. 10. In the case of samples with 100 μm thick layers (and one sample with a 35 μm thick layer), no subcritical crack growth was observed at measurable rates ($\geq 10^{-9}$ m/s) up to driving forces of ~ 200 J/m^2 .

As discussed above for the toughness behavior, moisture-assisted crack propagation only occurred by crack deviation off the interface into the alumina. Accordingly, as reasoned for the toughness results, the higher resistance to moisture-assisted crack propagation for samples with thicker aluminum layers is attributed to increased crack-tip plasticity and blunting that lowers the local crack-tip stresses relative to values necessary for the crack to leave the interface and enter the alumina. At 22 J/m^2 , where growth was first measured for 5 μm thick layer samples, the predicted σ_m/σ_0 ratio is greater than 7, while a sample with a 100 μm thick layer would need to be loaded to greater than 300 J/m^2 to experience similar stress levels ahead of the crack (Varias et al., 1991). At such high load

levels, only catastrophic fast fracture of the alumina is possible, and stable moisture-assisted crack growth cannot occur except possibly to aid in the initiation of crack extension into the ceramic.

Fig. 11 shows direct evidence that moisture-assisted crack growth was not occurring at the interface, with fatigue markings evident up to the point where the crack deviated into the alumina. The observed crack growth for the interface specimens was primarily intergranular in the alumina, and appeared to be identical to that observed in previous studies on moisture-assisted crack growth in bulk alumina (Evans, 1972; Freiman et al., 1974). For silica glass, it has been proposed that water molecules react with and rupture strained Si–O–Si bonds, leaving surface hydroxyl groups in the crack wake (Michalske and Freiman, 1983). Moisture-assisted crack growth in alumina is thought to occur by a similar mechanism along the glassy grain boundaries which, as in the present case for AD995 alumina, are commonly comprised of silica along with other sintering additives (e.g., CaO, MgO).

Initial moisture-assisted crack growth in the 5 μm thick layer samples occurred at driving forces lower than for crack growth in fatigue pre-cracked bulk alumina samples. It should be noted, how-

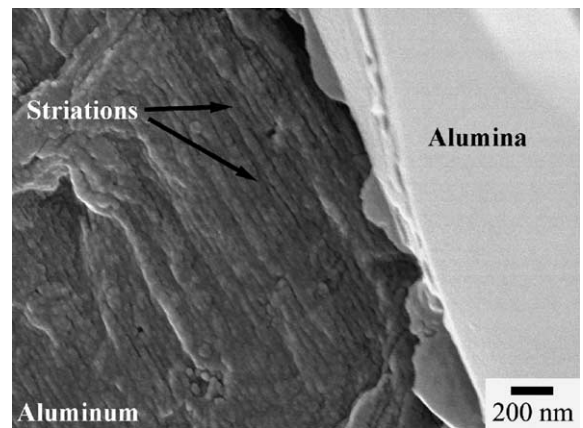


Fig. 11. Evidence of fatigue striations up to the point where the crack left the bimaterial interface during moisture-assisted crack growth. Direction of crack propagation was left to right with respect to the micrograph.

ever, that the curve shown for the bulk alumina is not unique, and only represents data from the initial growth from large (several millimeters) fatigue pre-cracks. Subsequent measurements of crack velocity (v - G) curves resulted in a shift of the data to higher driving forces, as illustrated in Fig. 12. Two v - G curves, measured in succession on the same sample at $\sim 40\%$ relative humidity, are shown in Fig. 12, where each measured curve is successively shifted to higher driving forces. This effect has been observed previously in alumina by Steinbrech et al. (1983), with the shifting of the v - G data attributed to the systematic progression up the R -curve. Indeed, if the contribution of crack shielding (e.g., grain bridging) could be accounted for, a v - G curve for the crack tip could be considered unique or intrinsic to the material (Lawn, 1993). Alternatively, an asymptotic curve for long-crack behavior could be developed where a steady-state bridging zone is achieved, as discussed above for crack growth under cyclic loading.

The marked shift of the v - G data to lower driving forces for the $5\ \mu\text{m}$ thick layer samples indicates that there was a lower initial starting

point on the alumina R -curve than for the fatigue pre-cracked bulk alumina samples, where initial pre-crack lengths were several millimeters in length. Indeed, initial crack growth for the $5\ \mu\text{m}$ thick layer samples occurred at a driving force of $22\ \text{J}/\text{m}^2$, which is very near the extrapolated initiation toughness of $\sim 20\ \text{J}/\text{m}^2$ taken from the R -curve shown in Fig. 4, where the fatigue pre-crack was only $230\ \mu\text{m}$ in length. The low driving force necessary for initial growth into the alumina for the $5\ \mu\text{m}$ thick layer samples implies an initial position near the beginning, or lowest point, of the alumina R -curve. Additionally, while care was taken to limit the data taken to the initial growth off the interface, a slight decrease in crack-growth rate with increasing driving force can be seen for the $5\ \mu\text{m}$ thick layer data in Fig. 10, which is attributed to the fact that some data were necessarily taken after progression up the R -curve, raising the driving forces necessary for crack extension. As was found in cyclic fatigue, the results indicate a crack size effect for globally large interface cracks that only begin to develop grain bridging, and subsequent R -curve toughening, after they deviate off the interface into the alumina.

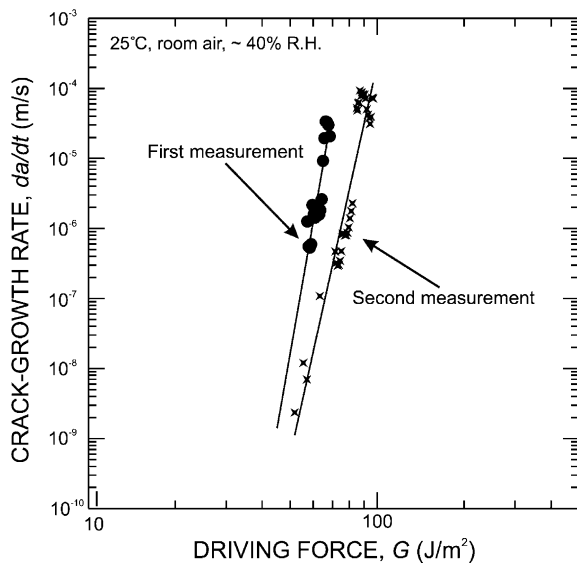


Fig. 12. Two sequentially measured v - G curves for a single fatigue pre-cracked bulk alumina sample measured in 40% relative humidity room air. The curve measured second is shifted to higher driving forces, corresponding to starting at a higher position on the alumina R -curve.

4. Conclusions

Based on an experimental study to investigate the effects of changing metal layer thickness (over the range from 5 to $100\ \mu\text{m}$) on the fracture and fatigue properties of the ceramic-metal $\text{Al}_2\text{O}_3/\text{Al}/\text{Al}_2\text{O}_3$ layered system, the following conclusions can be made:

1. The fracture toughness of the sandwich samples was seen to increase with increasing aluminum layer thickness. As the initial interfacial pre-cracks grew to fracture into the alumina, this trend was rationalized in terms of enhanced crack-tip deformation and blunting in the thicker metal layers (where plastic deformation is less constrained), which also lowered the local crack-tip stresses relative to those needed to trigger cracking at flaws in the alumina.
2. The interfacial fatigue-crack growth resistance was found to decrease with increasing

aluminum layer thickness at lower driving forces; this was observed in the form of lower fatigue thresholds and higher growth rates in the near-threshold regime. Stable cyclic fatigue-crack growth occurred predominantly at the $\text{Al}_2\text{O}_3/\text{Al}$ interface, except for 5 μm thick layer samples at higher driving forces. For the 100 μm thick layer samples, estimates of the plastic-zone size suggest that plasticity does not extend through the thickness of the layer at the fatigue threshold; for the 5 μm thick layer samples, conversely, the plasticity is constrained by the thickness of the layer, thereby limiting the degree of crack blunting and consequently the crack advance per cycle, even close to the threshold.

3. At higher driving forces, the trajectory of the cyclic fatigue cracks was found to change, specifically from an interfacial path to crack growth in the alumina, resulting in substantially less crack-growth resistance. While for thicker layers, growth into the alumina could only occur unstably (i.e., fast fracture), for 5 μm thick layer samples, stable cyclic fatigue-crack growth occurred in the ceramic. Additionally, “short-crack effects”, attributed to lack of grain bridging for a crack just entering the alumina, caused the initial cracking to occur at lower driving forces than normally measured for large cracks in bulk alumina.
4. Under static loads in a moist environment, cracks in samples with 5 μm thick metal layers also left the interface and propagated subcritically in the alumina; this did not occur in samples with 100 μm thick metal layers due to enhanced crack-tip blunting in the aluminum. Due to the lack of a crack-tip shielding zone of grain bridges in the interfacial crack wake, such initial crack growth into the alumina occurred at driving forces lower than that measured for crack growth from large fatigue pre-cracks in bulk alumina.
5. Whereas previous work has demonstrated that thinner metallic layers in alumina/aluminum structures produce higher strength ceramic/metal joints, the current study shows that although interfacial fatigue thresholds may also be improved, flaw tolerance is essentially re-

duced by lowering the overall fracture toughness and promoting subcritical crack growth off the interface and into the alumina. The latter phenomenon is observed under cyclic loading at high driving forces and under static loading in a moist environment.

Acknowledgements

This work was supported by the Director, Office of Science, Office of Basic Energy Sciences, Division of Materials Sciences and Engineering of the US Department of Energy under contract no. DE-AC03-76SF00098. The authors wish to thank Dr. Eric Stach and Doreen Ah Tye of the National Center for Electron Microscopy for help with the in situ FESEM work.

References

- Andreasen, J.H., Moller, C.V., Karihaloo, B.L., 1995. Fatigue crack growth from small surface cracks in transformation-toughened ceramics. *J. Am. Ceram. Soc.* 78, 406–410.
- Ashby, M.F., Blunt, F.J., Bannister, M., 1989. Flow characteristics of highly constrained metal wires. *Acta Metall.* 37, 1847–1857.
- Bennison, S.J., Lawn, B.R., 1989. Role of interfacial grain-bridging sliding friction in the crack-resistance and strength properties of nontransforming ceramics. *Acta Metall.* 37, 2659–2671.
- Cannon, R.M., Dalgleish, B.J., Dauskardt, R.H., Oh, T.S., Ritchie, R.O., 1991. Cyclic fatigue-crack propagation along ceramic/metal interfaces. *Acta Metall. Mater.* 39, 2145–2156.
- Card, J.C., Cannon, R.M., Dauskardt, R.H., Ritchie, R.O., 1993. Stress-corrosion cracking at ceramic–metal interfaces. In: Carim, A.H., Schartz, D.S., Silberglitt, R.S., Loehman, R.E. (Eds.), *Joining and Adhesion of Advanced Inorganic Materials*, vol. 314. Materials Research Society, pp. 109–116.
- Creager, M., Paris, P.C., 1967. Elastic field equations for blunt cracks with reference to stress corrosion cracking. *Int. J. Fract. Mech.* 3, 247–252.
- Dalgleish, B.J., Lu, M.C., Evans, A.G., 1988. The strength of ceramics bonded with metals. *Acta Metall.* 36, 2029–2035.
- Dalgleish, B.J., Saiz, E., Tomsia, A.P., Cannon, R.M., Ritchie, R.O., 1994. Interface formation and strength in ceramic–metal systems. *Scr. Metall. Mater.* 31, 1109–1114.
- Dalgleish, B.J., Trumble, K.P., Evans, A.G., 1989. The strength and fracture of alumina bonded with aluminum alloys. *Acta Metall.* 37, 1923–1931.

- Dauskardt, R.H., 1993. A frictional-wear mechanism for fatigue-crack growth in grain bridging ceramics. *Acta Metall. Mater.* 41, 2765–2781.
- Deans, W.F., Richards, C.E., 1979. A simple and sensitive method of monitoring crack and load in compact fracture mechanics specimens using strain gauges. *J. Test. Eval.* 7, 147–154.
- De Graef, M., Dalgleish, B.J., Turner, M.R., Evans, A.G., 1992. Interfaces between alumina and platinum: structure, bonding and fracture resistance. *Acta Metall. Mater.* 40, S333–S344.
- Elssner, G., Suga, T., Turwitt, M., 1985. Fracture of ceramic-to-metal interfaces. *J. Phys.* 46, C4-597–C4-612.
- Evans, A.G., 1972. A method for evaluating the time-dependent failure characteristics of brittle materials—and its application to polycrystalline alumina. *J. Mater. Sci.* 7, 1137–1146.
- Evans, A.G., Dalgleish, B.J., 1992. The fracture resistance of metal–ceramic interfaces. *Acta Metall. Mater.* 40, S295–S306.
- Evans, A.G., Lu, M.C., 1986. Some aspects of the mechanical strength of ceramic/metal bonded systems. *Acta Metall.* 34, 1643–1655.
- Evans, A.G., Dalgleish, B.J., He, M., Hutchinson, J.W., 1989. On crack path selection and the interface fracture energy in bimaterial systems. *Acta Metall.* 37, 3249–3254.
- Freiman, S.W., McKinney, K.R., Smith, H.L., 1974. Slow crack growth in polycrystalline ceramics. In: Bradt, R.C., Hasselmann, D.P.H., Lange, F.F. (Eds.), *Symposium of Fracture Mechanics of Ceramics*, vol. 2. Plenum, New York, NY, pp. 659–676.
- Gaudette, F., Suresh, S., Evans, A.G., 1999. The influence of solid-state and liquid-phase bonding on fatigue at Al/Al₂O₃ interfaces. *Metall. Mater. Trans. A* 30, 763–769.
- Gaudette, F., Suresh, S., Evans, A.G., Dehm, G., Rühle, M., 1997. The influence of chromium addition on the toughness of γ -Ni/ α -Al₂O₃ interfaces. *Acta Mater.* 45, 3505–3513.
- Geraghty, R.D., Hay, J.C., White, K.W., 1999. Fatigue degradation of the crack wake zone in monolithic alumina. *Acta Mater.* 47, 1345–1353.
- Gilbert, C.J., Han, Y.S., Kim, D.K., Ritchie, R.O., 2000. Anomalous cyclic fatigue-crack propagation behavior of small cracks in monolithic, grain bridging ceramics. *Ceram. Int.* 26, 721–725.
- Gilbert, C.J., Petrany, R.N., Ritchie, R.O., Dauskardt, R.H., Steinbrech, R.W., 1995. Cyclic fatigue in monolithic alumina: mechanisms for crack advance promoted by frictional wear of grain bridges. *J. Mater. Sci.* 30, 643–654.
- Gu, I., Ritchie, R.O., 1999. On the crack-tip blunting model for fatigue crack propagation in ductile materials. In: Panontin, T.L., Sheppard, S.D. (Eds.), *Fatigue and Fracture Mechanics*, vol. 29, ASTM STP 1332, West Conshohocken, PA, pp. 552–564.
- Guiu, F., Li, M., Reece, M.J., 1992. Role of crack-bridging ligaments in the cyclic fatigue behavior of alumina. *J. Am. Ceram. Soc.* 75, 2976–2984.
- Hay, J.C., White, K.W., 1993. Grain-bridging mechanisms in monolithic alumina and spinel. *J. Am. Ceram. Soc.* 76, 1849–1854.
- Healy, J., Bushby, A.J., Mai, Y.-W., Mukhopadhyay, A.K., 1997. Cyclic fatigue of long and short cracks in alumina. *J. Mater. Sci.* 32, 741–747.
- Hu, X., Mai, Y.-W., 1992. Crack-bridging analysis for alumina ceramics under monotonic and cyclic loading. *J. Am. Ceram. Soc.* 75, 848–853.
- Kishimoto, H., Ueno, A., Matsunaga, A., 1998. Cyclic-fatigue crack initiation and propagation in smooth alumina specimens. *J. Am. Ceram. Soc.* 81, 55–60.
- Korn, D., Elssner, G., Fischmeister, H.F., Rühle, M., 1992. Influence of interface impurities on the fracture energy of UHV bonded niobium–sapphire bicrystals. *Acta Metall. Mater.* 40, S355–S360.
- Kruzic, J.J., Campbell, J.P., Ritchie, R.O., 1999. On the fatigue behavior of γ -based titanium aluminides: role of small cracks. *Acta Mater.* 47, 801–816.
- Kruzic, J.J., Cannon, R.M., Ritchie, R.O., 2003. Crack-size effects on cyclic and monotonic crack growth in polycrystalline alumina: Quantification of the role of grain bridging. *J. Am. Ceram. Soc.* 86, in press.
- Lathabai, S., Rödel, J., Lawn, B., 1991. Cyclic fatigue from frictional degradation at bridging grains in alumina. *J. Am. Ceram. Soc.* 74, 1348–1360.
- Lawn, B., 1993. *Fracture of Brittle Solids*. Cambridge University Press, Cambridge, UK.
- Mai, Y.-W., Lawn, B.R., 1987. Crack-interface grain bridging as a fracture resistance mechanism in ceramics: II. Theoretical fracture mechanics model. *J. Am. Ceram. Soc.* 70, 289–294.
- McNaney, J.M., Cannon, R.M., Ritchie, R.O., 1994. Near-interfacial crack trajectories in metal–ceramic layered structures. *Int. J. Fract.* 66, 227–240.
- McNaney, J.M., Cannon, R.M., Ritchie, R.O., 1996. Fracture and fatigue crack growth along aluminum–alumina interfaces. *Acta Mater.* 44, 4713–4728.
- McNaney, J.M., Havens, R., Ritchie, R.O., 1997. Elastic compliance of the compact tension specimen comprising two linear-elastic materials bonded with a thin layer. *J. Test. Eval.* 25, 28–35.
- Michalske, T.A., Freiman, S.W., 1983. A molecular mechanism for stress corrosion in vitreous silica. *J. Am. Ceram. Soc.* 66, 284–288.
- Oh, T.S., Cannon, R.M., Ritchie, R.O., 1987. Subcritical crack growth along ceramic–metal interfaces. *J. Am. Ceram. Soc.* 70, C-352–C-355.
- Oh, T.S., Cannon, R.M., Rödel, J., Glaeser, A.M., Ritchie, R.O., 1988. Effects of near interfacial microstructure on toughness and subcritical crack growth in ceramic/metal systems. In: Ishida, H. (Ed.), *Interfaces in Polymer, Ceramic, and Metal Matrix Composites*. Elsevier, Amsterdam, pp. 567–581.
- Peralta, P., Ramamurty, U., Suresh, S., Campbell, G.H., King, W.E., Mitchell, T.E., 2000. Crystallographic effects on the

- fatigue fracture of copper–sapphire interfaces. *Philos. Mag. A* 80, 2109–2129.
- Reimanis, I.E., Dalglish, B.J., Brahy, M., Rühle, M., Evans, A.G., 1990. Effects of plasticity on the crack propagation resistance of a metal/ceramic interface. *Acta Metall. Mater.* 38, 2645–2652.
- Reimanis, I.E., Dalglish, B.J., Evans, A.G., 1991. The fracture resistance of a model metal/ceramic interface. *Acta Metall. Mater.* 39, 3133–3141.
- Ritchie, R.O., Yu, W., 1986. Short crack effects in fatigue: a consequence of crack tip shielding. In: Ritchie, R.O., Lankford, J. (Eds.), *Small Fatigue Cracks*. TMS-AIME, Warrendale, PA, pp. 167–189.
- Saxena, A., Hudak, S.J., 1978. Review and extension of compliance information for common crack growth specimens. *Int. J. Fract.* 14, 453–467.
- Shaw, M.C., Marshall, D.B., Dalglish, B.J., Dadkhah, M.S., He, M.Y., Evans, A.G., 1994. Fatigue crack growth and stress redistribution at interfaces. *Acta Metall. Mater.* 42, 4091–4099.
- Shih, C.F., Asaro, R.J., 1988. Elastic–plastic analysis of cracks on bimaterial interfaces: Part I—small scale yielding. *J. Appl. Mech.* 55, 299–316.
- Shih, C.F., Asaro, R.J., 1989. Elastic–plastic analysis of cracks on bimaterial interfaces: Part II—structure of small scale yielding fields. *J. Appl. Mech.* 56, 763–779.
- Steffen, A.A., Dauskardt, R.H., Ritchie, R.O., 1991. Cyclic fatigue life and crack-growth behavior of microstructurally small cracks in magnesia-partially-stabilized zirconia ceramics. *J. Am. Ceram. Soc.* 74, 1259–1268.
- Steinbrech, R., Blanke, H., Knehans, R., Schaarwächter, W., 1983. Crack kinetics of Al_2O_3 bend specimens with increasing crack resistance curves. In: Vincenzini, P. (Ed.), *Science of Ceramics*, vol. 12. National Research Council Research Institute for Ceramics Technology, Faenza, pp. 655–660.
- Steinbrech, R.W., Deuerler, F., Reichl, A., Schaarwächter, W., 1987. Correlation of crack opening displacement and crack resistance curve of alumina. In: Taylor, D., Davidge, R.W., Freer, R., Livey, D.T. (Eds.), *Science of Ceramics*, vol. 14. The Institute of Ceramics, Shelton, Stoke-on Trent, Staffs, UK, pp. 659–664.
- Suo, Z., Hutchinson, J.W., 1989. Sandwich test specimens for measuring interface crack toughness. *Mater. Sci. Eng. A* 107, 135–143.
- Suresh, S., Ritchie, R.O., 1984. Propagation of short fatigue cracks. *Int. Met. Rev.* 29, 445–476.
- Swanson, P.L., Fairbanks, C.J., Lawn, B.R., Mai, Y.-W., Hockey, B.J., 1987. Crack-interface grain bridging as a fracture resistance mechanism in ceramics: I. Experimental study on alumina. *J. Am. Ceram. Soc.* 70, 279–289.
- Turner, M.R., Evans, A.G., 1996. An experimental study of the mechanisms of crack extension along an oxide/metal interface. *Acta Mater.* 44, 863–871.
- Varias, A.G., Suo, Z., Shih, C.F., 1991. Ductile failure of a constrained metal foil. *J. Mech. Phys. Solids* 39, 963–986.
- Veerman, C.C., Muller, T., 1972. The location of the apparent rotation axis in notched bend testing. *Eng. Fract. Mech.* 4, 25–32.
- Wiederhorn, S.M., 1968. Moisture assisted crack growth in ceramics. *Int. J. Fract. Mech.* 4, 171–177.
- Zhang, Y.H., Edwards, L., 1996. Small, short, and long fatigue crack growth in an advanced silicon nitride ceramic material. *Scr. Mater.* 34, 1561–1566.